Carbon Trends 14 (2024) 100320

Contents lists available at ScienceDirect

Carbon Trends

journal homepage: www.elsevier.com/locate/cartre

Chemical degradation of magnesia–carbon refractories by different gaseous atmospheres

Marcos N. Moliné [a,*], Pablo G. Galliano [b], Analía G. Tomba Martinez [a]

[a] Instituto de Investigaciones en Ciencia y Tecnología de Materiales (INTEMA), CONICET-Facultad de Ingeniería/Universidad Nacional de Mar del Plata, Av. J.B. Justo 4302 (7600) Mar del Plata, Argentina
[b] Tenaris SIDERCA, DrSimini 250, 2804 Campana, Argentina

ARTICLE INFO

Keywords:
MgO-C refractories
Oxidation
Antioxidant
Graphite
Organic binder
Material applications

ABSTRACT

In this work, we use a novel methodology to analyse how the critical compositional variables of MgO—C bricks affect their chemical degradation by oxygen attack; the study focuses on the effect of the graphite content, the presence of aluminium, and the binder type. Oxidation tests are performed at 1000 °C, a typical preheating condition for steelmaking ladles, under two atmospheric conditions: one simulated the oxygen concentration in air, and the other, with a lower amount of oxygen, reproduces the conditions of the inner part of the brick when liquid steel is present. It was found that: a) the addition of Al reduces the carbon oxidation kinetic, mainly at a low O_2 partial pressure, b) increasing the graphite content led to a smaller decarburized area with higher O_2 consumption, and c) mixing CarboRes® with phenolic resin resulted in a higher O_2 consumption but at a slower oxidation rate.

1. Introduction

Magnesia–Carbon (MgO—C) refractories have been widely used in steel making industries as the main working lining brick material of electric arc furnaces, converters, and steel ladles, mainly because of its high refractivity, excellent thermal shock resistance, low wettability, and high slag penetration resistance [1–8].

Corrosion is the condition that most frequently limits the lifetime of these materials, due in part to the high service temperatures which favour chemical reactivity with the environment. Corrosion originates from the thermodynamic incompatibility between an external agent and the refractory components. For MgO—C bricks, these agents may be melts such as liquid metal or slags, and atmospheric gases, mainly O_2, CO, or CO_2 [7–14].

The susceptibility of refractories (MgO—C, Al_2O_3–C, Al_2O_3–MgO—C, etc.) to the attack of oxidising gases is mainly due to the carbon present in their composition, initially as graphite flakes composing the organic binder, and later as residual carbon as a consequence of the exposure of this binder to temperatures higher than ~ 250 °C. In other to enhance the oxidation resistance, different antioxidant additives have been included in the refractory composition, which acts by different mechanisms. The list of additives is rather extensive, including metals and alloys (Al, Si, Mg, Al-Si, Al-Mg, Al-Ca-Mg-Si), nitrides (Si_3N_4, AlN, h-BN), carbides (B_4C, Al_4SiC_4, $Al_8B_4C_7$, Al_4OC) and borides (ZrB_2, CaB_2) [15–21]. Nevertheless, aluminium is still the most common additive used as antioxidant for MgO—C bricks.

The carbon oxidation by external agents (usually atmospheric oxygen) is called “direct oxidation” (1–2), as opposed to carbothermal reduction, or “indirect oxidation” (3), which occurs in MgO—C materials via a solid-state reaction with other refractory components [6,7,11,12,22–24].

$$2\,C_{(s)} + O_{2(g)} \rightarrow 2\,CO_{(g)}\ (T > 500\ ^\circ C) \quad (1)$$

$$2\,CO_{(g)} + O_{2(g)} \rightarrow 2\,CO_{2(g)}\ (T > 1000\ ^\circ C) \quad (2)$$

$$MgO_{(s)} + C_{(s)} \rightarrow Mg_{(g)} + CO_{(g)}\ (T > 1400\ ^\circ C) \quad (3)$$

Direct oxidation has been extensively studied by different authors [4,11,13,24–29]; it has been established that it becomes critical above 700 °C in air and is determined by the diffusion of the gaseous species through the decarburised layer of the refractory. The oxidation resistance depends both on the composition and texture of the brick, including the purity and distribution of the raw materials, as well as on the partial pressure of O_2.

Until now, the reported studies have been limited almost exclusively

* Corresponding author.
E-mail address: marcosmoline@fi.mdp.edu.ar (M.N. Moliné).

https://doi.org/10.1016/j.cartre.2024.100320
Received 17 November 2023; Received in revised form 20 December 2023; Accepted 2 January 2024
Available online 4 January 2024
2667-0569/© 2024 The Authors. Published by Elsevier Ltd. This is an open access article under the CC BY-NC-ND license (http://creativecommons.org/licenses/by-nc-nd/4.0/).

to evaluating the material's reactivity to atmospheric air, with little exploration of other less oxidising conditions which occur during the material's service life in the steel industry, and which may have a similar effect on the loss of the carbonaceous component and consequently, on refractory integrity. In fact, only the hot face is directly exposed to air during preheating of the ladles, while the $O_{2(g)}$ pressure inside the wall may be lower, partly due to the dilution effect generated by the gases evolved in the reactions taking place in the refractory itself [30].

On the other hand, the effects of the typical compositional variables affecting the oxidation resistance of MgO—C bricks have been established, as is the case with the graphite or aluminium content; within certain limits, an increase in the graphite percentage, as well as the presence of the antioxidant, reduce the refractory's sensitivity to the attack by atmospheric air. However, there are variables that have still been ignored, such as the atmospheric composition, which hasn't been addressed in the literature thus far. In this work, we propose a systematic study of the influence of critical compositional variables—organic binder type, graphite content, and the addition of an antioxidant—on the ability of MgO—C bricks to resist attack by gaseous oxygen when it is present in different concentrations in the surrounding atmosphere. These conditions simulate the situations faced by bricks when used as steel ladle liners. In this way, the obtained results will serve not only to generate basic knowledge of aspects that have not yet been fully addressed or have not been completely solved, but also to create an impact on industrial practices. A specially designed methodology is used for this purpose [31], in which the oxidation process is monitored by determining the mass variation of the material and the oxygen concentration in the surrounding atmosphere.

2. Materials and methods

The bricks studied were specially designed but manufactured industrially using traditional pressing technology. Unlike most of the research reported in the literature, which has been carried out on laboratory-prepared materials, the use of industrially manufactured products facilitates the extrapolation of results to plant conditions.

The variables considered critical for this study were the graphite content (8 or 12 wt.%), the organic binder type (phenolic resin alone or mixed with a chemically modified pitch binder referred to as a "soft-binder" [32]), and the addition of an antioxidant additive (aluminium powder). The composition and designation of the materials are shown in Table 1. In every case, the major phase consists of fused and sintered magnesia particles (> 85 wt.%) incorporated in a mass ratio of 70:30, and the binder (~ 3 wt.%). A resol phenolic resin alone (bricks designated as R) or combined with a CarboRes® soft-binder in a 1:3 mass ratio (bricks designated as SB) were used as binders [32]. These bricks were extensively characterised, and the effect of the compositional differences on the characteristics of the as-received bricks have been previously published [33,34].

The evaluation of the performance of the different MgO—C refractories against by attack by different gaseous atmospheres was carried out with the methodology described in previous work by the authors [31], which consists of three main stages: 1) sample conditioning and characterisation, 2) treatment of the conditioned sample under thermal and atmospheric controlled conditions (oxidation test), and 3) tested material characterisation. During the oxidation test, the sample's mass and the variation in the oxygen concentration within its surrounding environment are monitored.

Table 1
Composition and label of MgO—C bricks.

Main components		SB8-0	SB8-A	SB12-0	R8-0
Weight percentage (wt.%)	Magnesia	89	87	85	89
	Graphite	8	8	12	8
	Aluminium	0	2	0	0
Organic binder (3 wt.%)		Resin + CarboRes®			Resin

2.1. Sample conditioning and characterisation

Cylindrical samples 26.6 mm in diameter and 25 mm in height cut from the refractory bricks were tested in a direction parallel to the pressing direction. The cylinder's flat faces were machined in order to maximise contact with the alumina discs that serve as sample holders [31], and to restrict their exposure to the gaseous atmosphere. Prior to the test, the samples were pyrolyzed in a graphite bed at 500 °C for 5 h (TT500) to eliminate organic volatiles. The material was characterised by measuring bulk density (ρ_b) and apparent porosity (π_a) according to DIN EN 993-1 [35]. Density was determined by pycnometry (ρ_{pyc}) on powdered samples (< 210 μm). In all cases, kerosene at 37 °C was used as the reference liquid along with a Sartorius BP 221 S balance. With these data, the true (or total) porosity (π_t) and the close porosity (π_c) were estimated. In addition, the carbon content was determined using the C LECO technique (CR12 LECO equipment) on powder samples (< 1 mm). The pore size distribution was determined to be within the range of 7.34 to 13,000 nm (mesopores) using a Pascal 440 Thermo Fisher Scientific mercury intrusion porosimeter on ~ 0.6 cm^3 samples.

2.2. Oxidation test

The evaluation of the gaseous corrosion of the materials was carried out at 1000 °C under two atmospheric conditions. The thermal condition was selected considering that this value is close to the temperatures reached by the hot face of the lining during the preheating of the steel ladle before receiving the liquid steel. Furthermore, most of the refractories in the ladle wall work at approximately 1000 °C in the successive filling and casting cycles [30,36].

The two atmospheric compositions were artificially generated by combining oxygen (purity: > 99.5 %) and argon (purity: 99.998 %) gases. In the more oxidising composition (Q-Ox), the amount of oxygen available in air was simulated (~ 20 vol.%); in the other condition (Q-Red), the oxygen concentration was reduced to values below 3 vol.%, thus simulating the condition of the inner part of the brick during the liquid steel's presence in the ladle. In this work, a synthetic mixture of gases was used to restrict the chemical attack to that coming from the reaction with gaseous O_2, thus avoiding the interaction with other gases present in the atmospheric air (such as in the case of nitrogen with aluminium). With these atmospheric conditions, different oxygen pressures to which the refractory lining are exposed during the ladle cycle were simulated, with the maximum being 20 vol.% O_2 in the composition of the prevailing atmosphere in contact with the working lining (hot face of the bricks) during the first preheating of the ladle [30,36].

Taking into account the temperature at which mass loss in the pyrolyzed materials begins (~ 600 °C, determined by TGA), only argon was blown from 500 °C onwards during heating and cooling under slight overpressure (1 to 1.1 atm). This was done to minimise the oxygen attack during both stages, thus favouring the flow of gases into the reactive chamber and limiting the ingress of atmospheric gases from the outside. The gases were injected with a total flow rate of 1 L/min during the dwell at 1000 °C. Under these regimes, the complete change of atmosphere in the reactive chamber was estimated to take ~ 3 min (~ 3 L at 1 L/min) [31].

2.3. Post-testing sample characterisation

Characterisation of the tested samples included variations in mass, apparent porosity, and bulk density. Textural parameters were determined in the same way as described above for the TT500 materials. In addition, the decarburised area was determined based on images of the cross sections obtained by performing a half-perpendicular cut relative to the specimen's axis after the sample was vacuum-packed with polyester resin. Photos of these sections are processed using Image-ProPlus

6.0 software.

3. Results and discussion

3.1. TT500 sample characterisation

The mass and carbon content variations of the TT500 samples (in percentage) are presented in Table 2. Considering that the mass loss corresponds mainly to volatiles coming from the pyrolysis of the organic binder, the percentage of residual carbon was estimated as the difference between the mass variation and the binder content estimated by TGA (carried out under air flow); both values are included in the same table [33,34].

It is confirmed that adding CarboRes® to the organic binder composition generates a higher carbon yield (more residual carbon), which is ~ 65 % for SB bricks and ~ 55 % for the brick bonded with only phenolic resin; moreover, the amount of total carbon was found to be higher in SB8-0 than in R8-0 after treatment at 500 °C (TT500).

The textural parameters of the TT500 materials are shown in Table 3 compared with the values of the original materials (O). The bulk density (ρ_b) was found to be correlated with the pycnometric density (ρ_{pyc}) in both the TT500 and original materials. The latter parameter increased in all cases after heat treatment at 500 °C, in agreement with the condensation undergone by the organic binder when pyrolysis occurs, the volatiles are eliminated, and the residual carbon is formed. The values of apparent (π_a), closed (π_c) and true (π_t) porosities increased in all cases after the thermal treatment.

The increase in the fraction of open pores is associated with both the loss of solid material in the form of volatile species and the formation of channels for their escape, as indicated by the fact that the increase in the parameter π_a does not follow the variation in mass during the heat treatment (Table 3). The generation of open pores was less severe in the refractory with aluminium, which can be associated with the fact that the initial apparent porosity was already higher, so it was not necessary to generate such a high number of new channels for the escape of volatiles. It is interesting to note that the proportion of closed pores after the heat treatment also increased, with SB12-0 being the material in which this change was most noticeable.

The modification to the type of organic binder did not produce significant differences with respect to the increase in apparent and closed porosity, and SB8-0 and R8-0 reached similar π_a values after treatment at 500 °C despite the fact that data in Table 2 show that the quantity of mass removed during the 500 °C treatment was lower in the resin-bonded material. On the other hand, the closed porosity exhibited by the R8-0 TT500 material was higher than that of SB8-0 TT500, as was the total porosity (π_t). The differences between the mechanisms by which pyrolysis occurs in the phenolic resin, the semi-coke, and the original pitch (the latter two phases present in CarboRes®) could have caused the differences in π_t and π_c of the pyrolyzed SB and R refractories.

The distributions of pore sizes smaller than 13 μm (mesopores) for the TT500 samples are shown in Fig. 1 together with the original brick's curves. In addition, the contribution to pore volume of specific size ranges is reported in Table 4.

The pore size distributions are more similar among the four pyrolyzed materials in comparison with the as-received bricks. The TT500 samples had, in general, a greater portion of pores smaller than 3 μm, which is associated with the formation of channels through which the volatiles could escape. The curves for SB8-0 and SB8-A after treatment at 500 °C were similar (as were the bricks in their original condition), and there was also a similarity in apparent porosity (Table 4).

The material with the highest graphite content (SB12-0) did not present significant differences in the evaluated pore size distribution before and after the pyrolyzing treatment, highlighting the contribution of pores < 1 μm with respect to the rest of materials. The refractory bonded with only phenolic resin (R8-0) showed the greatest variation in the distribution of small pores (< 13 μm) with respect to the original brick. In addition, it presented a greater contribution of pores < 1 μm with respect to SB8-0

Open pores smaller than ~ 10 μm (related to the interparticle spaces) are those which most influence the refractory's permeability, and fluid penetration occurs through pores that are larger than ~ 1 μm in this type of material [37–41]. Taking this information into account, an analysis of the pore size distributions allows us to estimate an order of permeability among the studied materials.

According to the parameters obtained after TT500, the addition of aluminium to the brick's composition generates a material with an apparent porosity volume similar to SB8-0 TT500, even in the range of sizes < 1 μm. Considering these characteristics, a significant difference in permeability between SB8-A and SB8-0 due to thermal effects would not be expected, although there are other factors that affect this parameter, such as the pores' degree of interconnectivity (related to the apparent-to-true porosity ratio, which is somewhat lower in SB8-A TT500).

The lower apparent porosity (π_a, Table 3) of the SB12-0 TT500 material with respect to SB8-0 TT500 and the high amount of pores < 1 μm suggest that the permeability would be lower for the former. Moreover, it is estimated that the permeability of R8-0 TT500, whose apparent porosity is similar to that of SB8-0 TT500 but with a higher percentage of pores smaller than 1 μm, is lower than that of this latter material. The lower degree of interconnectivity that could be expected between the pores of R8-0 TT500 with respect to that of SB8-0 TT500 (apparent porosity/true porosity is 0.48 and 0.66, respectively) contributes to support this hypothesis.

Regarding the carbon content after TT500, a slight decrease was observed in SB8-0 and SB8-A (~ 3 % and 8 %, respectively), which can be attributed mainly to residual C removal. The loss of this carbonaceous material could be related to the higher permeability inferred for these refractories after TT500, which are also the materials that lost more mass during the thermal treatment [33,36,42]. In SB12-0 and R8-0, on the other hand, a slight increase in the carbon content (3 % and 7 %, respectively) was observed after TT500, which could be attributed to soot formation. This solid is produced from gaseous CO under low oxygen partial pressure conditions [36,42] ($2CO_{(g)} \rightarrow CO_{2(g)}$ y $C_{(s)}$). The CO gas may be a product of the incomplete oxidation of the graphite in the bed or the C in the refractory itself. Coincidentally, SB12-0 TT500 and R8-0 TT500 have the highest percentage of small pores (and lower permeability according to the above-mentioned estimation), which may be due to the deposition of soot, and also lose less mass during the thermal treatment (Table 2). The formation of this type of could also be responsible for the high closed porosity of R8-0 after TT500 (π_c, Table 3) since the deposit of this solid can block the pores [36]. The degree of pore interconnectivity provides additional support to the soot formation hypothesis since it decreases in every case with the thermal treatment, especially for SB12-0, and less so for SB8-0 and SB8-A.

Table 2
Mass and carbon content variation after treatment at 500 °C.

	Mass variation (wt. %)	Residual carbon (wt.%)	Total carbon (wt. %)		Residual carbon (wt.%)
			Original	TT500	
SB8-0	−1.51 ± 0.06	4.4	10.2	9.9	2.89 ± 0.06
SB8-A	−1.56 ± 0.06	4.2	10.0	9.2	2.64 ± 0.06
SB12-0	−1.39 ± 0.05	4.2	13.0	13.4	2.81 ± 0.05
R8-0	−1.28 ± 0.09	3.0	8.6	9.2	1.72 ± 0.09

3.2. Oxidation test

The variations in the samples' mass and the oxygen concentrations, which were determined in one of the tests carried out at 1000 °C for each of the MgO—C (pyrolyzed) refractories in both atmospheres, are shown

Table 3
Textural parameters of the as-received and TT500 materials.

	ρ_{pyc}[1] (g/cm^3)		ρ_b[2](g/cm^3)		π_a[3](%)		π_t[4] (%)		π_c (%)	
	O	TT500	O	TT500	O	TT500	O	TT500	O	TT500
SB8-0	3.24	3.45	3.05	3.10	3.4	6.7	4.8	10.1	~ 1.4	~ 3.4
SB8-A	3.22	3.51	2.97	3.10	5.6	6.3	7.7	11.7	~ 2.1	~ 5.4
SB12–0	3.10	3.32	2.94	2.97	4.1	5.5	5.1	10.5	~ 1.0	~ 5.0
R8-0	3.30	3.60	3.08	3.12	3.6	6.4	6.7	13.3	~ 3.1	~ 6.9

Standard deviation:.
[1] ± 0.04.
[2] ± 0.05.
[3] ± 0.03.
[4] ± 0.02.

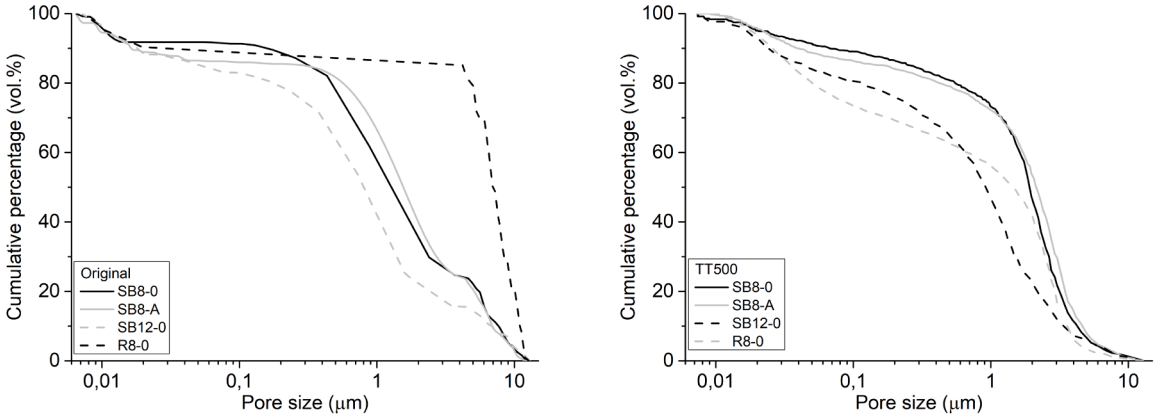

Fig. 1. Cumulative pore size distribution of the original MgO—C bricks (a) and TT500 samples (b).

Table 4
Discretized pore size distribution in the original (O) and TT500 materials.

Materials	Percentage (vol.%)							
	< 0.02 μm		0.02–1 μm		1–3 μm		3–13 μm	
	O	TT500	O	TT500	O	TT500	O	TT500
SB8-0	8.1	4.9	34.6	23.1	30.3	50.3	27.0	21.7
SB8-A	11.0	5.4	22.9	22.4	38.7	42.6	27.4	29.6
SB12-0	11.6	7.3	46.8	46.9	24.1	33.8	17.5	12.0
R8-0	9.8	6.0	3.7	38.0	1.1	39.2	85.4	16.8

in Fig. 2. The maximum differences obtained between duplicates were ± 0.1 % for both the mass and oxygen concentrations (except for the mass loss during the heating of SB8-0, which was less than ± 0.2 %), which shows very good reproducibility for oxidation test. The graphs showing how the oxygen concentration evolved also include the "reference run", which corresponds to a test performed under the same atmospheric, temperature, and time conditions, but without the refractory sample [31].

The sample's mass variation, net losses in all cases, shows differences in the reaction rate among the evaluated MgO—C bricks. Comparatively, the four materials showed similar behaviour in both reaction atmospheres. Mass losses were less than 1 wt.% and 0.1 wt.% during heating and cooling, respectively.

The mass losses after the thermal dwell are reported in Table 5 (1000 °C, 1 h), together with the total values recorded at the end of the test and those obtained by the difference between the sample's mass before and after testing. The mean average corrosion rate, estimated as the mass loss with respect to the exposed lateral area of the cylindrical specimens and the exposure time (1 h), is also reported. Considering that the mass loss during the test was mainly due to carbon oxidation by atmospheric oxygen, the amount of this component consumed in the test was estimated by taking into account the total amount of carbon determined in the TT500 samples (C LECO in Table 2); the values in percentage are shown as 'C loss' in Table 5.

The results in Table 5 show that even in the most oxidising condition (Q-Ox), the available carbon was not completely consumed in any of the cases, with the maximum consumption being close to 35 % for the R8-0 brick (which has less carbon than the rest of the materials and is among the less permeable ones). In this condition, the material with Al (SB8-A) consumed the lowest amount of carbon during the test (~ 15 %).

In Q-Ox, the refractory with Al lost mass more slowly than the reference material SB8-0 (~ 3 g/m^2.min with respect to ~ 5 g/m^2.min); at the end of the dwell time at 1000 °C, the mass loss in SB8-A was ~ 60 % of the value recorded for SB8-0. In contrast, the brick with phenolic resin as a binder (R8-0) and the material with more graphite (SB12-0) lost mass more quickly than SB8-0 (~ 7 g/m^2.min and ~ 9 g/m^2.min, respectively) in the oxidising atmosphere; the difference with the reference refractory was more pronounced for SB12-0, which exhibited the fastest mass variation among the four bricks. At the end of the dwell time at 1000 °C, the mass loss was ~ 30 % and 60 % higher for R8-0 and SB12-0, respectively, than that of SB8-0. Similar differences, although

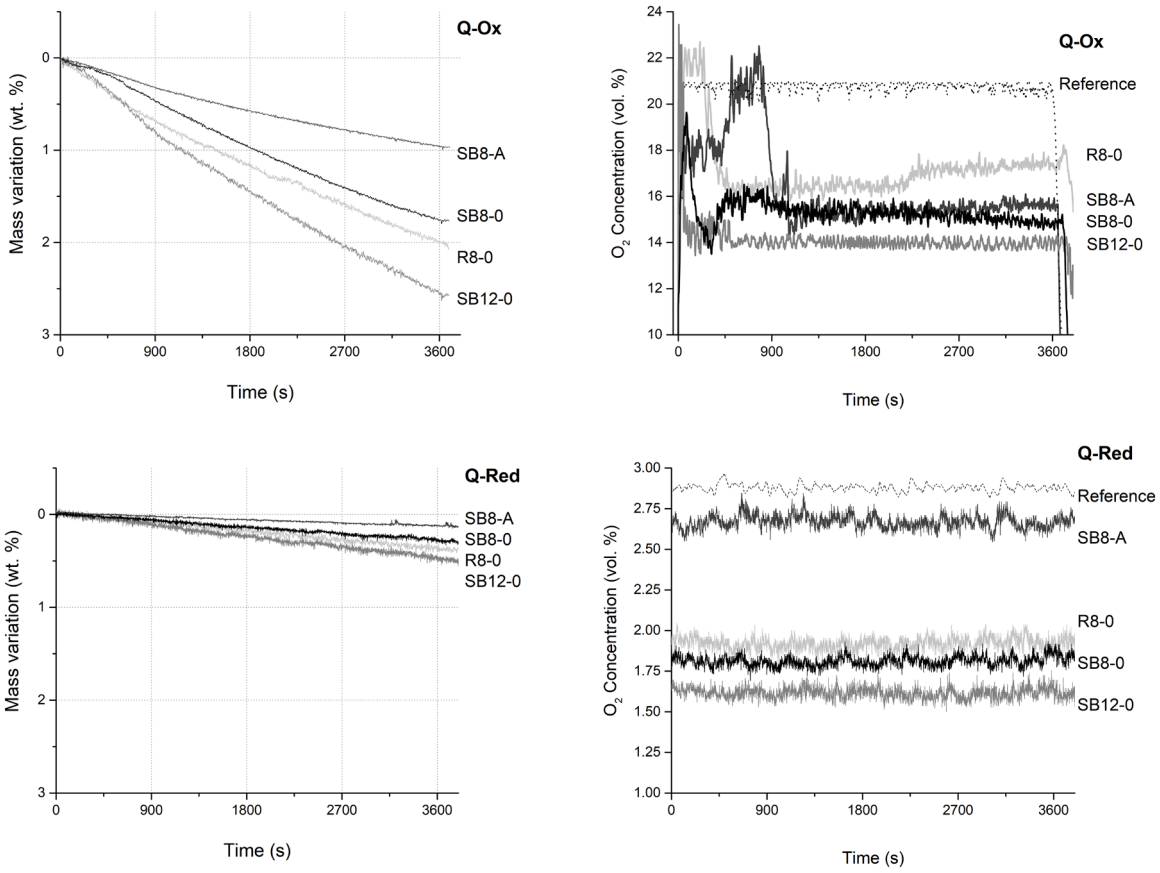

Fig. 2. Variation of the sample's mass and oxygen concentrations during treatments of MgO—C (pyrolyzed) materials in Q-Ox and Q-Red atmospheres at 1000 °C (1 h).

Table 5
Mean mass losses and oxidation rate of MgO—C materials.

	Condition	1000 °C, 1 h			Total		
		Mass loss[1] (wt.%)	C loss[2] (wt. %)	Rate (g/ m^2. min)	Mass loss[1] (wt.%)	C loss[2] (wt. %)	Mass loss[3] (wt.%)
SB8-0	Q-Ox	1.59	16.1	5.1	2.40	24.2	2.43
	Q-Red	0.38	3.7	1.2	1.07	10.8	1.08
SB8-A	Q-Ox	1.01	11.0	3.2	1.44	15.7	1.48
	Q-Red	0.14	1.5	0.5	0.49	5.3	0.51
SB12-0	Q-Ox	2.65	19.8	8.5	3.90	29.1	4.20
	Q-Red	0.50	3.8	1.6	1.75	13.1	1.75
R8-0	Q-Ox	2.17	23.6	6.9	3.18	34.6	3.12
	Q-Red	0.37	4.0	1.2	1.44	15.7	1.38

[1] Standard deviation: ± 0.03 %.
[2] Percentage of consumed carbon estimated as: (Mass loss/ TT500 total carbon)*100.
[3] Difference between the sample's mass determined before and after testing.

smaller in magnitude, were recorded in the atmosphere with only 3 vol. % O_2.

The reference runs show that the oxygen concentration reached a constant value of ~ 2.8 vol.% during the dwell time at 1000 °C in Q-Red, and ~ 20.9 vol.% in Q-Ox [31]. Considering the partial pressure of each gas (argon and oxygen) in the mixture and the flow rate of 1 L/min used during 60 min at 1000 °C, it was estimated that the total amount of injected O_2 moles were 0.56 in Q-Ox and 0.075 in Q-Red (assuming ideal gas behaviour) [31]. With these data, the oxygen consumption in each test was estimated by the difference between the total injected amount and the value given by the area under the O_2 concentration curve (Fig. 2). These values are reported in Table 6. The O_2 consumption was always higher in the more oxidising atmosphere, although the percentage of oxygen consumed with respect to the injected amount was higher in Q-Red (30–40 % with respect to 20–30 %), with the exception of SB8-A.

The oxygen consumption during the dwell time at 1000 °C was practically constant in the Q-Red tests, while in the more oxidising atmosphere it exhibited a significant variation along the thermal dwell (Fig. 2). Regarding the evolution of the oxygen concentration in Q-Ox, SB8-0 seemed to consume it from the beginning of the gas injection, so much so that the maximum O_2 concentration (at ~ 1.5 min after the onset of the permanence at 1000 °C) did not reach the value determined in the reference run (19.6 vol.% compared to 20.9 vol.%). After ~ 8 min, the rate of oxygen consumption slowed down (~ 16 vol.% of O_2 still remained in the system) and slowly decreased until the end of the test. Something similar occurred with SB-A, but more slowly, since the O_2 concentration continued increasing after the first 1.5 min up to the reference value at ~ 8 min from the beginning of the dwell; subsequently, the oxygen concentration dropped to a constant value of ~ 15.5 vol.%. These two (pyrolyzed) materials appear to be the most permeable of the set, thus justifying the high initial oxygen consumption.

In the tests of SB12-0 and R8-0 which, on the contrary, have lower initial permeability and a higher amount of soot deposition, the oxygen concentration has the maximum value—which corresponded to the reference run value (20.9 vol.% O_2)—at the beginning of the gas injection. In particular, SB12-0 started to consume oxygen immediately and maintained the reference run value for only a few seconds, after which the O_2 concentration dropped sharply below the value reached in the rest of the materials, down to ~ 14 vol.%. On the other hand, R8-0 showed the longest delay in reacting with the oxygen present in the

Table 6
Estimated oxygen consumption during the oxidation tests.

O_2 Consumption	SB8-0		SB8-A		SB12-0		R8-0	
	Q-Ox[2]	Q-Red[3]	Q-Ox	Q-Red	Q-Ox	Q-Red	Q-Ox	Q-Red
(mol)	0.146	0.027	0.125	0.008	0.185	0.030	0.095	0.025
(% mol)[1]	26.1	36.0	22.3	10.7	33.0	40.0	17.0	33.3

Standard deviation:.
[1] ± 0.5 %
[2] ± 0.003 %
[3] ± 0.001 %

gas mixture since the O_2 concentration remained at the maximum level (20.9 vol.%) for at least 4 min, after which it dropped down close to 16 vol.%. Subsequently, the oxidation rate was significantly reduced, and less and less oxygen was consumed during the rest of the dwell time at 1000 °C.

The decarburised area of the tested refractory samples is reported in Table 7 together with the textural parameters. The percentage variation with respect to the values of the pyrolyzed samples (TT500, Table 2) is reported in parentheses.

The oxidation processes generated an increase in the apparent porosity in every material, with increases of more than 78 % in Q-Ox (except for SB8-A), and significantly smaller increases in Q-Red. These results were accompanied by a slight decrease in bulk density in all cases, which is related to the increase in porosity.

The variations in the estimated oxygen consumption, the decarburised area, and the increase in apparent porosity as a function of the total carbon loss (considering that the mass loss is a product of the oxidation of this component, Table 5) are shown in Fig. 3 for the two studied atmospheres. The four refractories presented comparatively similar behaviours in Q-Ox and Q-Red, since the same relative order is observed for the each of the indicators of the oxidation process in both atmospheric conditions.

On the one hand, it is expected that the greater the oxygen consumption, the greater the carbon loss, as observed for the three SB materials. R8-0, which contained only phenolic resin as an organic binder, did not follow the same trend: more carbon was oxidised than that in SB8-0, but less oxygen was consumed. The effect is more noticeable in Q-Ox, where oxygen consumption was as low as that estimated in the refractory with the antioxidant. Likewise, it is expected that higher carbon consumption involves an increase in the decarburised area, as found in the three materials with 8 wt.% of graphite. However, this did not occur in the SB12-0 material, which, together with SB8-A, exhibited the lowest values of this parameter in both atmospheric conditions despite its high oxygen and carbon consumption. Finally, the increase in apparent porosity correlated adequately with the degree of carbon oxidation for the four MgO—C refractories, as can be seen in Fig. 4, although the R8-0 material deviated from the general trend, especially in Q-Red.

Table 7
Decarburised area and textural parameters of the MgO—C tested materials.

	Test	Decarburised area (%)	Bulk density (g/cm^3)	Apparent porosity (%)	
SB8-0	Q-Ox	37.4 %	3.00 ± 0.05	11.9 ± 0.2	(+78 %) [1]
	Q-Red	15.2 %	3.08 ± 0.02	8.0 ± 0.2	(+19%)
SB8-A	Q-Ox	23.9 %	2.96 ± 0.05	9.7 ± 0.2	(+54 %)
	Q-Red	13.1 %	3.08 ± 0.03	6.5 ± 0.2	(+3 %)
SB12-0	Q-Ox	24.1 %	2.87 ± 0.07	10.1 ± 0.2	(+84 %)
	Q-Red	12.9 %	2.93 ± 0.04	6.7 ± 0.2	(+22 %)
R8-0	Q-Ox	41.7 %	2.97 ± 0.04	13.1 ± 0.2	(+105 %)
	Q-Red	21.4 %	3.01 ± 0.08	10.2 ± 0.2	(+60 %)

[1] Variation of the parameters with respect to the apparent porosity of the materials TT500 (π_a, Table 3).

3.3. Effect of compositional variables

3.3.1. Antioxidant

With respect to SB8-0, the added antioxidant (SB8-A) was the only compositional variable that produced a reduction in carbon loss during the dwell time at 1000 °C in both atmospheric conditions (from 16 % to 11 % wt. % in Q-Ox and from 4 to 1 wt.% in Q-Red); the effect was more noticeable in the less oxidising atmosphere. Correlatively, both the estimated O_2 consumption and the decarburised area were reduced when Al is present (a reduction of ~ 15 % in Q-Ox and ~ 70 % in Q-Red for the first indicator, and ~ 40 % in Q-Ox and ~ 10 in Q-Red in the second) and the apparent porosity was less affected, especially in the Q-red (the variation decreased from 78 % to 54 % in Q-Ox and from 19 % to 3 % in Q-Red with the metal added). The effect of the antioxidant was not only reflected in the above indicators, which all together show a clear decrease in the amount of carbon oxidised during the test, but also in the slowing down of the reaction with gaseous O_2, as was previously discussed.

In the evaluated thermal range, aluminium can improve the material's resistance to oxidation by gaseous oxygen via different mechanisms, such as its higher affinity for O_2 than carbon and the filling of pores with the reaction's products. As previously discussed, the permeability of SB8-0 TT500 and SB8-A TT500 would be similar, and no very distinct differences in O_2 availability at the onset of the reaction would be expected between both refractories. Under oxidising conditions, if Al reacts faster than C with O_2 forming Al_2O_3, there will be a delay in mass loss, as was observed in Fig. 2, and a decrease in the amount of O_2 available to oxidise C. This explains why oxygen was consumed from the onset of the gas injection in the case of SB8-0, but then, the oxygen concentration varied more gradually than in the reference material due to the competition of both oxidative processes. The abrupt drop in oxygen concentration at ~ 15 min could indicate that the Al closer to the sample's surface reacted completely, after which oxygen consumption evolved similarly to SB8-0, reacting exclusively with carbon, as observed in Fig. 2. The slope change in the mass evolution at ~ 15 min after the onset of the thermal dwell, coincident with that determined for the O_2 concentration, reinforces this theory.

When there is a lower percentage of oxygen (Q-Red), the oxidative process in SB8-A occurred in a similar manner, but the Al was not completely consumed in the reaction zone during the thermal dwell at 1000 °C due to the low availability of oxidising gas; this was inferred from the oxygen consumption curve, which does not show a significant drop, and the absence of any change in the rate of the mass variation (Fig. 2). The difference between the decarburised areas of SB8-A and SB8-0 was smaller in Q-Red than in Q-Ox. This may be caused by the low probability of contact between O_2 and C or Al particles due to the low concentration of the gas when Ar-3 vol.% O_2 was used as the reactive atmosphere; in this conditions, the oxygen becomes the limiting reactive

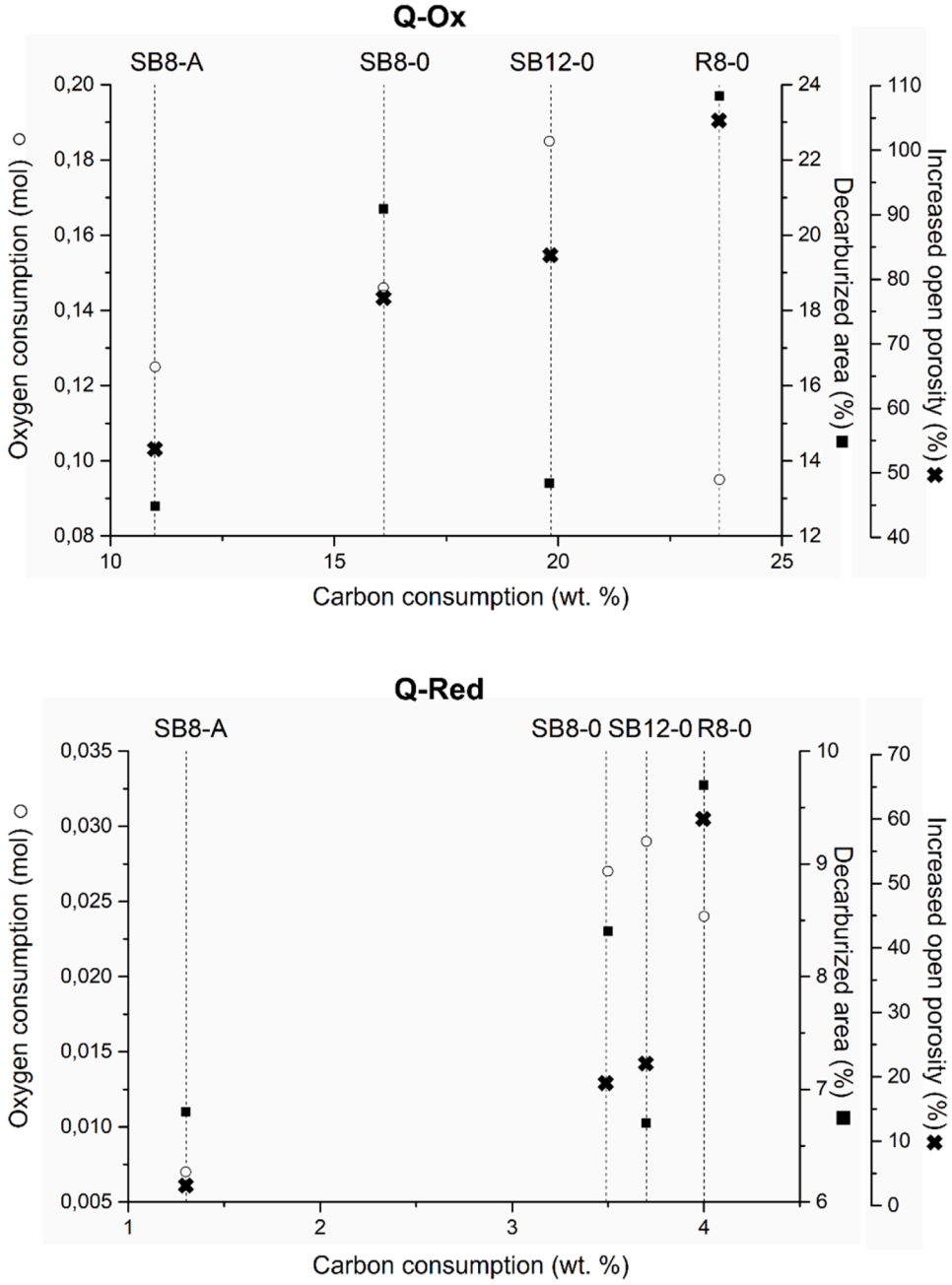

Fig. 3. Oxygen consumption, decarburised area, and apparent porosity increase as a function of the carbon consumption in the oxidation tests.

for both type of materials, in spite of their compositions, reducing the difference in the amount of oxidized carbon between SB8-0 and SB8-A with respect to the oxidant condition.

The solid product created by the antioxidant's reaction with O_2 can fill the pores contributing to the smaller increase in apparent porosity experienced by SB8-A with respect to the rest of the materials. This fact gives support to the hypothesis about the limiting role of the oxygen under O-Red conditions, since a large difference would be expected in the decarburized area between SB8-0 and SB8-A taking into account the lower amount of channels for gas penetration created in the latter.

3.3.2. Graphite

The increase in graphite content present in the original composition (SB12-0 material) involved higher carbon loss and oxygen consumption with respect to SB8-0: 20 % higher in Q-Ox and < 5 % in Q-Red for the first parameter, while 27 % and 11 % more oxygen was consumed in Q-Ox and Q-Red, respectively. However, the higher proportion of graphite in the original refractory did not translate into an increase in the decarburised area; conversely, this area was reduced by 35 % in Q-Ox, and 15 % in Q-Red with respect to SB8-0. Furthermore, the increase in apparent porosity was lower than would be expected taking into account the other oxidation indicators (C and O_2 consumption), especially under oxidising conditions (from 78 % in SB8-0 to 84 % in SB12–0 under more oxidising conditions, and from 19 % to 22 % in Q-Red).

The differences between the oxidation indicators determined in SB12-0, which deviate from those expected in comparison with SB8-0, could be related, on the one hand, to the greater resistance impeding the gas from penetrating the material (due to its lower permeability). On the other hand, the behaviour of SB12-0 could be due to the presence of a higher amount of soot deposited during the previous heat treatment at 500 °C, which is surely the carbonaceous component most susceptible to oxygen attack. The soot oxidation justifies the abrupt drop in oxygen

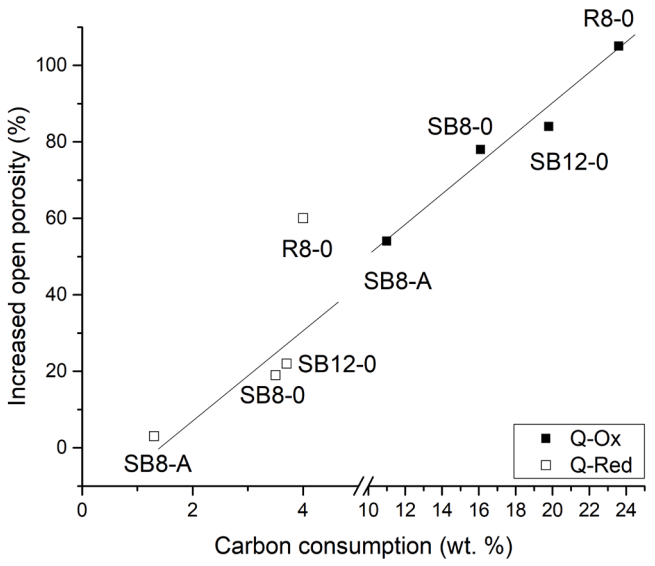

Fig. 4. Increase in apparent porosity in tested MgO—C materials as a function of carbon consumption.

concentration and the faster mass loss during the tests of SB12-0 in Q-Ox, compared to SB8-0; after depleting this carbon source, only the residual carbon and the remaining graphite would be oxidised, which seems to occur at a similar rate to that of SB8-0 (in agreement with the estimated O_2 consumption). The faster soot oxidation generated a high concentration of gaseous products, whose diffusion towards the outside impeded the entry of reactive gases into the refractory sample more effectively, further reducing the decarburised area. The differences between the results when the material was exposed to a lower oxygen concentration (Q-Red) is also explained by the higher susceptibility of the soot present in SB12-0, which made the material more sensitive to oxygen, producing a higher consumption of this gas.

3.3.3. *Organic binder*

The use of phenolic resin as the only organic binder (R8-0) produced, with respect to SB8-0, higher carbon loss, a larger decarburised area, and an increase in apparent porosity as a consequence of the thermal treatment, but with a lower oxygen consumption in both environmental conditions. By comparing the oxidation indicators of R8-0 and SB8-0, it is evident that these effects were even more marked in less oxidising conditions (Q-Red): a) carbon losses were ~ 40 % higher in Q-Ox, and ~ 10 % in Q-Red, b) decarburised areas were higher by ~ 15 % in Q-Ox and ~ 40 % in Q-Red c). Furthermore, apparent porosity increased by ~ 35 % in Q-Ox and ~ 200 % in Q-Red. On the other hand, R8-0 consumed ~ 35 % less oxygen in Q-Ox than SB8-0, and ~ 7 % less in Q-Red.

Several factors can be analysed in the comparison between SB8-0 and R8-0. The lower permeability inferred for R8-0 TT500 with respect to that of SB8-0 TT500, which would have a significant effect restricting the reactive gases from entering the sample's interior, was not a determining factor since decarburisation progressed more in this sample than in the rest of the materials; however, it could still be the cause of the delay that was observed at the onset of oxidation in this brick (Fig. 2). Other factors to be considered are the higher proportion of soot formed in this material during TT500 (this refractory exhibited the highest increase in C content, Table 2) and the higher susceptibility to oxidation exhibited by the residual carbon formed by the resin pyrolysis (due to its low degree of organization, [32–34]). This higher sensitivity signifies that a lower oxygen concentration is needed to produce a certain level of oxidation in comparison with that required by the refractory that also contains CarboRes®, resulting in a lower total O_2 consumption. The slope change observed in the oxygen concentration variation during the dwell at 1000 °C in Q-Ox (Fig. 2)—which is also present in the mass loss curve—can be attributed to the residual carbon consumption.

Soot loss, which was considered as a possible cause of pore blockage in R8-0 TT500, would result in the opening of those (closed) pores, leading to a greater increase in the final apparent porosity. The fact that there are components in the brick's composition that are more sensitive to being oxidised can explain why some of the differences between the oxidation indicators are more pronounced in Q-Red when compared to SB8-0 (as explained for the case of the SB12–0 material).

3.4. *Impact of the results on in-service performance*

Considering the use of MgO—C bricks as linings for steelmaking ladles, the results obtained in the tests carried out at different oxygen concentrations allow us to anticipate how the evaluated compositional variables affect the bricks in service.

Regarding the addition of aluminium, its effect and the improvement it provides to the brick's oxidation resistance will be more noticeable in the interior of the refractory wall during the ladle preheating than at the working face. This situation would also help maintain the antioxidant effect within the wall's interior throughout the campaign. Since the hot face undergoes partial wear after each casting, it is also important that the face subsequently exposed to the next empty ladle preheating cycle receive some of the protection provided by the Al or its reaction products.

The results obtained in the oxidation tests show that the increase in graphite content did not translate into a larger decarburised area, and the increase in porosity was less than expected, especially under oxidising conditions. For this reason, having more graphite in the brick's composition will reduce the risk of losing material during subsequent casts due to steel and slag attack. Although more C is consumed by its reaction with oxygen when more graphite is present in the refractory's composition, the greater volume of gaseous products (CO) slows the progress of oxidation within the brick.

Compared to the brick containing CarboRes®, the low oxidation resistance exhibited when only phenolic resin is used as a binder will reduce its useful life, not only during the first heating, but throughout the entire campaign of the lining because the innermost refractory wall, where oxygen pressure drops down, suffers even greater deterioration.

Finally, the results obtained suggest that the deposition of a by-product such as soot due to the reaction of the CO generated by the carbon oxidation present in the bricks themselves in the low temperature regime (< 700 °C) could be beneficial. The presence of this type of carbon reduces the apparent porosity and the subsequent graphite consumption, thus showing how important it is to minimise its removal by virtue of the role this component plays in the brick's performance. Therefore, it is convenient to take into account the occurrence of this process when designing the preheating thermal cycle; if the oxidation can be controlled at the beginning, the formation of soot may help improve the subsequent lining performance.

4. Conclusions

As a result of the main changes that occur in the materials during their thermal treatment in a graphite bed at 500 °C (volatiles are eliminated and channels are created for the gases to escape), there was an increase in the volume of open and closed pores and a larger percentage of pores smaller than 3 μm. The textural parameters of the pyrolyzed materials were less different than those of the original bricks.

The results of the characterisation of the materials thermally treated at 500 °C suggest that there was a deposition of soot formed by the reaction of the CO generated in the atmosphere, mainly in those bricks with a higher graphite content (SB12-0) or bonded with only resin as a binder (R8-0). According to the global analysis of the data obtained for the pyrolyzed materials, SB8-0 and SB8-A have similar permeability, which is greater than the permeability of SB12-0 and R8-0 when subjected to the same treatment.

The use of aluminium as an antioxidant substantially improved the oxidation resistance of the refractory material (SB8-A with respect to SB8-0) at 1000 °C, which was manifested in the lower carbon losses and the lower amount of open pores formed, together with a reduction in the rate of the reaction with oxygen. This behaviour, more marked for the lower concentration of O_2 in the atmosphere, was attributed to the preferential oxidation of Al over C, and to the possible filling of pores by the reaction product (alumina).

Increasing the graphite content in the brick from 8 to 12 wt.% reduced the oxidation reaction's progress towards the interior of the material, although the carbon consumption was faster and higher, with these effects being more noticeable in a more oxidising environment. The response of SB12-0 compared with that of SB8-0 was related to its lower permeability, which restricted the oxidising gas' penetration into the material (after pretreatment at 500 °C), and to the formation of soot, which is the first carbonaceous substance to be consumed.

The addition of CarboRes® to the phenolic resin had a beneficial effect on the oxidative behaviour, as evidenced by the lower reactivity of SB8-0 over R8-0. This was manifested in the lower decarburisation and slower oxidation rate of the former despite its higher estimated oxygen consumption; the differences between SB8-0 and R8-0 were more marked in the less-oxidising atmosphere. The addition of CarboRes® (SB8-0) alters the residual carbon formed after binder pyrolysis, thus promoting a greater degree of order in the structure; as a result, this carbon's behaviour in relation to the gaseous oxygen will be more similar to that of graphite than the fully amorphous carbon formed by the resin pyrolysis, making it more resistant to direct oxidation.

CRediT authorship contribution statement

Marcos N. Moliné: Writing – original draft, Visualization, Validation, Software, Methodology, Investigation, Formal analysis, Data curation, Conceptualization. **Pablo G. Galliano:** Writing – review & editing, Validation, Supervision, Resources, Project administration, Conceptualization. **Analía G. Tomba Martinez:** Writing – review & editing, Supervision, Resources, Project administration, Methodology, Investigation, Funding acquisition, Data curation, Conceptualization.

Declaration of competing interest

The authors declare that they have no known competing financial interests or personal relationships that could have appeared to influence the work reported in this paper.

Data availability

Data will be made available on request.

Acknowledgements

This work was supported by the Agencia Nacional de Promoción Científica y Tecnológica (ANPCyT) of Argentina under the projects: "Degradación química de refractarios de uso siderúrgico", PICT 2012 N°1215 and "Estudios orientados al tratamiento de problemáticas relacionadas a la fabricación y propiedades en servicio de refractarios óxido-C para la industria del acero" PICT 2017 N° 2482. It was also carried out within the scope of the CYTED network 312RT0453 (HOREF). The authors would like to thank Ing. N. Bellandi for providing the refractory bricks.

References

[1] M. Bakhtiari, R. Emadi, A. Monshi, Effects of ferrosilicon addition and formation of insitu SiC nano-whiskers on MgO-C refractories, 14 (2017) 38–43.

[2] L.L. Snead, D.T. Hoelzer, M. Rieth, A.A.N. Nemith, Chapter 13 - Refractory Alloys: Vanadium, Niobium, Molybdenum, Tungsten, Elsevier Inc., 2019, https://doi.org/10.1016/B978-0-12-397046-6.00013-7.

[3] S. Biswas, D. Sarkar, Introduction to refractories for iron- and steelmaking, 2020. doi:10.1007/978-3-030-43807-4.

[4] D. Ding, L. Lv, G. Xiao, J. Luo, C. Lei, Y. Ren, S. Yang, P. Yang, X. Hou, Improved properties of low-carbon MgO-C refractories with the addition of multilayer graphene/MgAl2O4 composite powders, Int. J. Appl. Ceram. Technol. 17 (2020) 645–656, https://doi.org/10.1111/ijac.13347.

[5] Y. Cheng, T. Zhu, Y. Li, S. Sang, Microstructure and properties of MgO–C refractory with different carbon contents, Ceram. Int. 47 (2021) 2538–2546, https://doi.org/10.1016/j.ceramint.2020.09.099.

[6] M. Ludwig, E. Śnieżek, I. Jastrzębska, R. Prorok, M. Sułkowski, C. Goławski, C. Fischer, K. Wojteczko, J. Szczerba, Recycled magnesia-carbon aggregate as the component of new type of MgO-C refractories, Constr. Build. Mater. (2021) 272, https://doi.org/10.1016/j.conbuildmat.2020.121912.

[7] M. Raju, S.C. K, T. Mahata, D. Sarkar, H.S. Maiti, Improvement in the properties of low carbon MgO-C refractories through the addition of graphite-SiC micro-composite, J. Eur. Ceram. Soc. 42 (2022) 1804–1814, https://doi.org/10.1016/j.jeurceramsoc.2021.11.049.

[8] X. Wang, C. Deng, J. Di, G. Xing, J. Ding, H. Zhu, C. Yu, Enhanced oxidation resistance of low-carbon MgO–C refractories with Al3BC3–Al antioxidants: a synergistic effect, J. Am. Ceram. Soc. 106 (2023) 3749–3764, https://doi.org/10.1111/jace.19023.

[9] W.E. Lee, S. Zhang, Melt corrosion of oxide and oxide-carbon refractories, Int. Mater. Rev. 44 (1999) 77–104.

[10] M. Chen, S. Gao, L. Xu, N. Wang, High temperature mechanical and corrosion resistance of Fe-containing MgO-C refractory in oxidizing atmosphere, Ceram. Int. 45 (2019) 21023–21028, https://doi.org/10.1016/j.ceramint.2019.06.306.

[11] J. Xiao, J. Chen, Y. Wei, Y. Zhang, S. Zhang, N. Li, Oxidation behaviors of MgO-C refractories with different Si/SiC ratio in the 1100–1500 °C range, Ceram. Int. 45 (2019) 21099–21107, https://doi.org/10.1016/j.ceramint.2019.07.086.

[12] Y. Liu, Q. Wang, G. Li, J. Zhang, W. Yan, A. Huang, Role of graphite on the corrosion resistance improvement of MgO–C bricks to MnO-rich slag, Ceram. Int. 46 (2020) 7517–7522, https://doi.org/10.1016/j.ceramint.2019.11.250.

[13] Z. Liu, J. Yu, S. Yue, D. Jia, E. Jin, B. Ma, L. Yuan, Effect of carbon content on the oxidation resistance and kinetics of MgO-C refractory with the addition of Al powder, Ceram. Int. 46 (2020) 3091–3098, https://doi.org/10.1016/j.ceramint.2019.10.010.

[14] Q. Wang, F. Tan, Z. He, G. Li, J. Li, Quantitative evaluation of slag corrosion on MgO-C refractory by experimental and numerical simulation, Miner. Met. Mater. Soc 73 (2021) 2709–2714, https://doi.org/10.1007/s11837-021-04793-w.

[15] A.P. Luz, V.C. Pandolfelli, Review Article: performance of the antioxidants in carbon containing refractories, Ceramica 53 (2007) 334–344, https://doi.org/10.1590/s0366-69132007000400002.

[16] C.G. Aneziris, J. Hubálková, R. Barabás, Microstructure evaluation of MgO-C refractories with TiO_2- and Al-additions, J. Eur. Ceram. Soc. 27 (2007) 73–78, https://doi.org/10.1016/j.jeurceramsoc.2006.03.001.

[17] A.S. Gokce, C. Gurcan, S. Ozgen, S. Aydin, The effect of antioxidants on the oxidation behaviour of magnesia – carbon refractory bricks, Ceram. Int. 34 (2008) 323–330, https://doi.org/10.1016/j.ceramint.2006.10.004.

[18] C. Atzenhofer, H. Harmuth, Phase formation in MgO-C refractories with different antioxidants, J. Eur. Ceram. Soc. 41 (2021) 7330–7338, https://doi.org/10.1016/j.jeurceramsoc.2021.07.023.

[19] J. Chen, Y. Du, Y. Zhang, M. Nath, W. Yan, Y. Wei, S. Zhang, N. Li, Oxidation behaviors of low carbon MgO-C refractories: roles of Ti 2 AlC and Ti 2 AlN, J. Am. Ceram. Soc. (2023) 4411–4424, https://doi.org/10.1111/jace.19100.

[20] Z. Liu, C. Deng, C. Yu, J. Ding, H. Zhu, Improving the anti-oxidation and water wettability of graphite through the design of coating structure for the preparation of Al2O3–SiC–C castables, Ceram. Int. 49 (2023) 29104–29113, https://doi.org/10.1016/j.ceramint.2023.06.186.

[21] Y. Luo, X. Wang, Z. Liu, C. Yu, C. Deng, J. Ding, Enhanced oxidation resistance and thermal shock resistance of low-carbon Al2O3–C refractories with nano-BN: a synergistic of mullitization behavior, J. Alloys Compd. 975 (2024) 172937, https://doi.org/10.1016/j.jallcom.2023.172937.

[22] O. Senneca, Oxidation of carbon: what we know and what we still need to know, Energy Procedia 120 (2017) 62–74, https://doi.org/10.1016/j.egypro.2017.07.155.

[23] B.M. Thethwayo, J.D. Steenkamp, A review of carbon-based refractory materials and their applications, J. South. Afr. Inst. Min. Metall. 120 (2020) 641–650, https://doi.org/10.17159/2411-9717/1011/2020.

[24] R. Kundu, R. Sarkar, MgO-C Refractories : A Detailed review of these irreplaceable refractories in steelmaking, (2021) 46–55.

[25] X. Li, M. Rigaud, S. Palco, Oxidation kinetics of graphite phase in magnesia-carbon refractories, J. Am. Ceram. Soc. 78 (1995) 965–971, https://doi.org/10.1111/j.1151-2916.1995.tb08423.x.

[26] N.K. Ghosh, D.N. Ghosh, K.P. Jagannathan, Oxidation mechanism of MgO-C in air at various temperatures, Br. Ceram. Trans. 99 (2000) 124–128, https://doi.org/10.1179/096797800680839.

[27] M.A. Faghihi-Sani, A. Yamaguchi, Oxidation kinetics of MgO-C refractory bricks, Ceram. Int. 28 (2002) 835–839, https://doi.org/10.1016/S0272-8842(02)00049-4.

[28] S. Hu, R. Zhu, R. Liu, K. Dong, Decarburisation behaviour of high-carbon MgO-C refractories in O2-CO2 oxidising atmospheres, Ceram. Int. 44 (2018) 20641–20647, https://doi.org/10.1016/j.ceramint.2018.08.056.

[29] S.S. Nair, T. Saha, P. Dey, S. Bhadra, Thermal oxidation of graphite as the first step for graphene preparation: effect of heating temperature and time, J. Mater. Sci. 56 (2021) 3675–3691, https://doi.org/10.1007/s10853-020-05481-x.
[30] P.G. Galliano, C.E. Cicutti, The impacts of corrosion damage - effect of ladle lining refractory on steel quality. Corros. Refract. Impacts Corros., Göller Verlag GmbH, Germany, 2018, pp. 343–374.
[31] M.N. Moliné, P.G. Galliano, A.G. Tomba Martinez, A novel methodology for evaluating high temperature gas corrosion of oxide-C refractories, Ceram. Int. 49 (2023) 19273–19280, https://doi.org/10.1016/j.ceramint.2023.03.054.
[32] C.L. Pássera, L.B. Manfredi, A.G. Tomba Martinez, Study of the thermal behavior of organic binders used in oxide-carbon refractory bricks, Metall. Mater. Trans. B. 52 (2021) 1681–1694.
[33] M.N. Moliné, S.E. Gass, P.G. Galliano, A.G. Tomba Martinez, The effects of binder type combined with graphite content and the presence of aluminum on the characteristics of MgO–C bricks, Ceram. Int. 48 (2022) 34627–34634, https://doi.org/10.1016/j.ceramint.2022.08.050.
[34] S.E. Gass, W.A. Calvo, M.N. Moliné, P.G. Galliano, A.G.T. Martinez, Combined effects of the graphite content and addition of aluminum in the characteristics of resin-bonded MgO-C bricks, Mater. Today Commun. 30 (2022), https://doi.org/10.1016/j.mtcomm.2021.103057.
[35] DIN EN 993-1, DIN 51056 - Method of test for dense shaped refractory products. Determination of bulk density, apparent porosity and true porosity., (1995).
[36] S.E. Gass, P.G. Galliano, A.G. Tomba Martinez, Impact of preheating on the mechanical performance of different MgO-C bricks—Intermediate temperature range, J. Eur. Ceram. Soc. 41 (2021) 3769–3781, https://doi.org/10.1016/j.jeurceramsoc.2021.01.025.
[37] M.D.M. Innocentini, V.C. Pandolfelli, Permeable porosity of refractory castables evaluated by the water-expulsion porosimetry technique, J. Am. Ceram. Soc. 84 (2001) 236–238, https://doi.org/10.1111/j.1151-2916.2001.tb00640.x.
[38] Y. Xu, S. Sang, Y. Li, B. Ren, L. Zhao, Y. Li, S. Li, Pore structure, permeability, and alkali attack resistance of Al 2O3-C Refractories, Metall. Mater. Trans. A Phys. Metall. Mater. Sci. 45 (2014) 2885–2893, https://doi.org/10.1007/s11661-014-2217-1.
[39] S. Shaobai, R. Bo, X. Yibio, L. Yawei, Improvement of gaseous corrosion resistance of refractories by pore structure design according to the seepage flow model, WorldForum 8 (2016) 111–117.
[40] N. Nishiyama, T. Yokoyama, Permeability of porous media: role of the critical pore size, J. Geophys. Res. Solid Earth. 122 (2017) 6955–6971, https://doi.org/10.1002/2016JB013793.
[41] W.A. Calvo, P. Ortega, M.J. Velasco, V. Muñoz, P. Pena, A.G.T. Martinez, Characterization of alumina-magnesia-carbon refractory bricks containing aluminium and silicon, Ceram. Int. 44 (2018) 8842–8855, https://doi.org/10.1016/j.ceramint.2018.02.069.
[42] S.K. Sadrnezhaad, S. Mahshid, B. Hashemi, Z.A. Nemati, Oxidation mechanism of C in MgO-C refractory bricks, J. Am. Ceram. Soc. 89 (2006) 1308–1316, https://doi.org/10.1111/j.1551-2916.2005.00863.x.